Strength and Frequency Analysis of the Lower Arm of a Double Wishbone Suspension of a Passenger Car

Stiliyana Taneva
Department of Transport and Aircraft Equipment and Technologies
Technical University of Sofia, Plovdiv Branch
Plovdiv, Bulgaria
s.taneva@tu-plovdiv.bg

Krasimir Ambarev
Department of Transport and Aircraft Equipment and Technologies
Technical University of Sofia, Plovdiv Branch
Plovdiv, Bulgaria
kambarev@tu-plovdiv.bg

Stanimir Penchev
Department of Transport and Aircraft Equipment and Technologies
Technical University of Sofia, Plovdiv Branch
Plovdiv, Bulgari
spenchev@tu-plovdiv.bg

Abstract. **One of the main elements of the suspension system is the lower control arm, which serves to transmit horizontal forces from the wheels to the chassis, while also defining the nature of the wheel movements relative to the chassis and the road surface. The implementation of guiding, elastic, and damping devices requires a comprehensive modelling of the vehicle's motion during the design stage. This paper presents results from static strength analysis and frequency analysis of the lower control arm of an independent front double-wishbone suspension of a passenger car. For this purpose, a three-dimensional geometric model of the lower control arm was created, using the Honda Civic as a prototype for the passenger car. The loads under various operating conditions necessary for conducting static analysis were determined. The Finite Element Analysis (FEA) was employed using the Simulation module of the SolidWorks software to solve the problem. Stresses, displacements, natural frequencies, and modes of the control arm were determined. The results were compared with experimentally obtained data for the natural frequencies.**

Keywords: experimental study, FEA, natural frequency and mode shape, rubber bushing, strength analysis.

I. Introduction

Suspension systems play a crucial role in reducing dynamic loads on vehicle bodies and wheels by mitigating shocks and vibrations. They often adjust the position of the vehicle chassis.

One of the primary challenges in car suspensions involves the distribution of stresses during vehicle movement, along with managing the magnitude of vibrations.

It is widely recognized that optimal driving comfort is attained when the natural frequency falls within the range of 1-1.5 Hz. In real-world vehicle applications, natural frequencies fluctuate between 0 to 20 Hz due to road imperfections [1].

Studies [2]-[4] provide results regarding various analysis of the suspension system using modern software tools.

The control arm of the suspension has been the subject of investigation in several studies [1], [5]-[14]. Specifically, research [7], [9], [14] has focused on static strength and frequency calculations of the suspension arm using FEA with different software platforms. During the suspension design phase, emphasis is placed on the geometry, mass, and individual components, prompting numerous studies [6], [7], [10], [11] dedicated to the structural and topology optimization of the arm. Additionally, various dynamic analyses of suspension components, including the lower arm, have been conducted through numerical and experimental studies as outlined in [1], [4], [5], [8], [13].

The aim of this study is to present a static strength analysis and frequency analysis of the lower control arm in an independent front double-wishbone suspension system of a passenger car. To achieve this objective, a three-dimensional geometric model of the lower control arm was developed using SolidWorks, with the Honda Civic serving as a prototype. FEA was employed to conduct simulations, and the natural frequencies obtained were experimentally validated as part of the study.

II. MATERIALS AND METHODS

A. Determination of the forces

For light vehicles with front suspension, MacPherson struts, double wishbone, and multi-link suspensions are most commonly used. The main advantage of the double-arm suspension is that by selecting the lengths and spatial positions of the arms, minimal change in the angle of their side inclination and convergence can be achieved during wheel lift and drop. The load-bearing capacity of the double-arm suspension is high, and it can be applied to all types of vehicles.

Fig. 1 represents the kinematic scheme of the double wishbone suspension, with the Honda Civic passenger car used as a prototype.
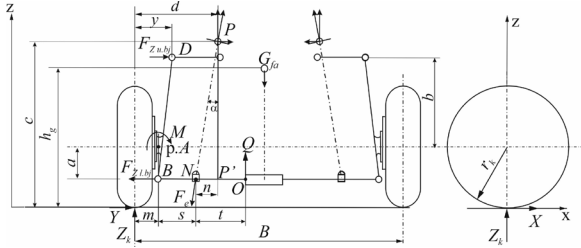

Fig. 1. Scheme of a double wishbone suspension.

To determine the initial conditions for simulating the suspension, the forces acting during characteristic load cases of vehicle movement were predefined. These include acceleration with maximum intensity, lateral loading, and dynamic loading when overcoming on road obstacles.

The static load on a front wheel is determined by the formula

$$Z_k = \frac{m_{fa}}{2}.g \quad , N \quad , \tag{1}$$

where m_{fa} is the mass of the front axle of the vehicle, [kg]; g is acceleration due to gravity, $g = 9{,}81$ m/s^2.

The maximum driving force on the wheel (acceleration with maximum intensity) is determined according to the relationship [15]

$$X_{\max} = \varphi.\xi_a.Z_k \quad , N \tag{2}$$

where φ is the grip coefficient on dry asphalt road; ξ_a is the weight distribution coefficient for the specified axle during acceleration is assumed, and for the front axle: $\xi_a = 0{,}8 \div 0{,}9$.

The maximum braking force on the wheel is calculated according to the relationship [15]

$$X_{c\max} = \varphi.\xi_b.Z_k \quad , \tag{3}$$

where ξ_b is the weight distribution coefficient for the specified axle during braking, for the front axle: $\xi_b = 1{,}1 \div 1{,}2$.

The maximum lateral force for the inner and outer wheels is determined according to the relationships [15]

$$Y_{\max in.wheel} = \varphi.Z_k \left(1 - \varphi \frac{2.h_g}{B} \right), \tag{4}$$

$$Y_{\max out.wheel} = \varphi.Z_k \left(1 + \varphi \frac{2.h_g}{B} \right), \tag{5}$$

where h_g is the height of the vehicle's center of gravity; B is the track width of the axle.

The maximum value of the lateral force Y is the greater of the two.

The dynamic load on the wheel when overcoming individual obstacles is determined according to the relationship [15]

$$Z_{max} = k_d . Z_k , \tag{6}$$

where k_d is the dynamic coefficient for vehicles primarily moving on flat, hard-surfaced roads $k_d = 1{,}5$-$2{,}1$.

The forces in the supports and joints caused by the normal, lateral (transverse), longitudinal reactions, and dynamic loading are determined, with reduction to point A in force and moment (fig.1). The forces acting on the shock absorber are not considered because the scheme is analyzed statically.

The main dimensions of the suspension, necessary for the calculations, are presented in Table 1.

The proper adjustment of supports is crucial for determining the stress displacement, natural frequencies, and mode shapes of both the suspension and the arm. The static stiffness of rubber bushings can be determined through mathematical equations, FEA, or experimental methods.

TABLE 1 GEOMETRIC PARAMETERS OF THE SUSPENSION.

Parameter	Designation	Value
Mass of the front axle	m_{fa}	885.5 kg
Radius of the wheel	r_k	0.27 m
Front axle track width	B	1.475 m
Height of the center of gravity	h_g	0.524 m
Coefficient of grip normal/during braking	φ	0.8/0.6
Parameters based on the fig. 1.	m	0.040 m
	s	0.120 m
	t	0.270 m
	a	0.115 m
	b	0.380 m
	y	0.150 m
	d	0.3 m
	c	0.7 m
	n	0.075 m
	α	7°50'

B. Methodology of study

The focus of this study is the lower arm of the double wishbone front independent suspension installed on the Honda Civic passenger car. Fig. 2 illustrates a 3D model of the lower arm. The geometric representation of the lower arm primarily includes two arms - longitudinal and transverse, bolted joints, three rubber bushings, and a component for attachment to the frame. Each geometric

detail of the arm is individually modeled and subsequently assembled to form the complete unit.
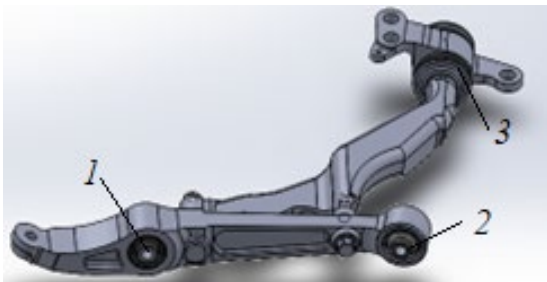

Fig. 2. Three-dimensional geometric model of a lower arm: 1, 2 and 3 – rubber bushings.

The strength calculation of the lower arm was conducted under static loading in three typical scenarios: maximum braking force (Case I), maximum lateral force (Case II), and maximum force encountered when the car overcomes single obstacles (Case III). Table 2 provides the values of the forces necessary for the strength calculations. These forces were oriented and designated relative to a coordinate system situated within the hole where the ball joint is installed. The strength analysis was performed utilizing the geometric model of the lower arm, excluding the rubber bushings and ball joint.

TABLE 2 FORCES OF THE LOWER ARM.

Option	Forces, N		
	X -axis	*Y -axis*	*Z -axis*
I	351	4343	3764
II	6601	4343	-
III	702	8687	-

Rubber bushings were employed as elastic supports for the lower arm. The proper definition of their fixing was determined based on the stiffness results of the rubber bushings obtained from a separate study by the same authors.

The lower arm is assembled from five distinct components, which two arms are made of cast carbon steel and the bolted joints – alloy steel, according to EN 1.0406. Their mechanical properties were shown in Table 3.

TABLE 3 MECHANICAL PROPERTIES OF THE LOWER ARM DETAILS.

Properties	Cast carbon steel	Alloy steel
Elastic modulus, MPa	200000	210000
Poisson's ratio	0.32	0.28
Mass density, kg/m³	7800	7700

Fig. 3 shows arm fixation established by elastic supports on the mounting locations on the surface of the rubber bushings.
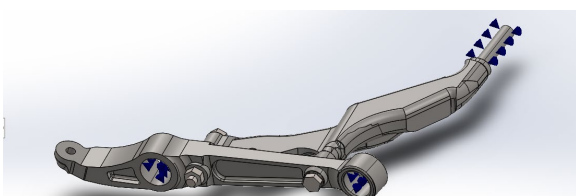

Fig. 3. Elastic supports.

Fig. 4 shows the load on the lower arm during braking (Case I). The other loads are implemented in a similar way.
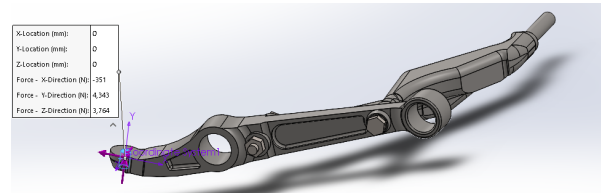

Fig. 4. Loads of the lower arm – Case I.

A three-dimensional curvilinear mesh was generated (fig. 5). It includes 86578 nodes and 53845elements.
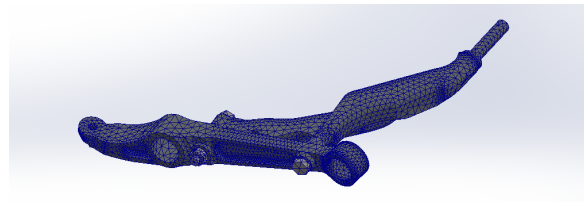

Fig. 5. FEA mesh.

The frequency analysis was performed by fixation as in the strength analysis.

The natural frequencies of the lower arm were also obtained by conducting a physical test. The experimental study was carried out by using a developed system for determining the natural frequencies presented in [16,17].

Fig. 6 shows the object, and the measuring equipment for the experiment.

Fig. 6. Experimental determination of natural frequencies.

The accelerometer was attached to the arm. The mass of the accelerometer is 1,27 g while the mass of the arm is approximately 7200 g. The total mass of the accelerometers on the suspension arm has negligible effects on the measurement. The FFT method in the Matlab software was used.

III. RESULTS AND DISCUSSION

Table 4 presents the results of the stiffness obtained via FEA, which are necessary for conducting the lower arm analyses.

TABLE 4 FEA STATIC STIFFNESS OF THE RUBBER BUSHINGS.

Stiffness	Values		
	Rubber bushing 1	*Rubber bushing 2*	*Rubber bushing 3*
Axial stiffness (N/mm)	460.5	234.1	376.9
Radial stiffness (N/mm)	5014	1743.4	3959

A. Static strength analysis results

The following figures show some of the obtained results of the numerical study, which include equivalent stress and absolute displacement.
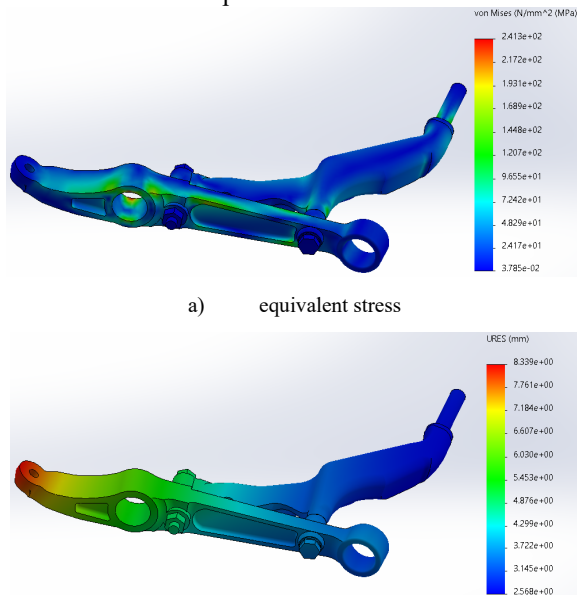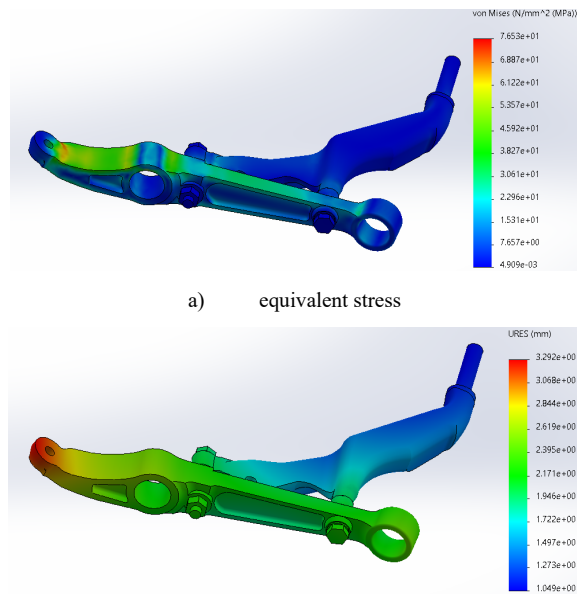

a)   equivalent stress

b)   absolute displacement

Fig. 7. Result for load Case I

a)   equivalent stress

b)   absolute displacement

Fig. 8. Result for load Case II

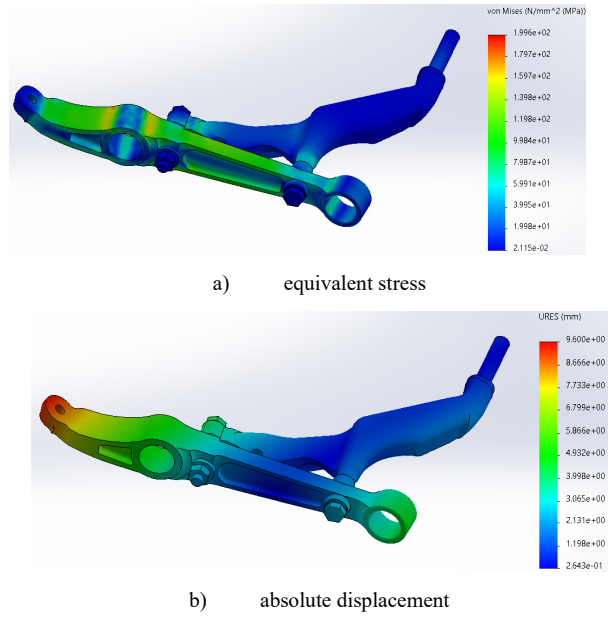a)   equivalent stress

b)   absolute displacement

Fig. 9. Result for load Case III

Among the three considered variants of static strength analysis, the highest values of the obtained stresses are observed in load Case I, with a maximum value of around 241 MPa.
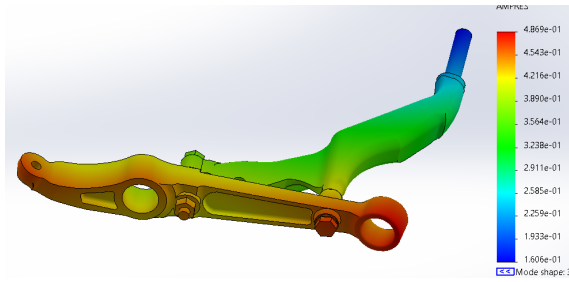
B. Frequency analysis results

Table 5 presents the obtained results of the six natural frequencies from FEA of the lower arm. The first, second and third mode shapes were shown on Fig. 10 a, b and c, respectively.

TABLE 5 NATURAL FREQUENCY FROM FEA.

Mode number	Natural Frequency, Hz
1	61.8
2	129.9
3	134.1
4	160.5
5	162.6
6	267.4

a)   first mode shape

b)   second mode shape

355
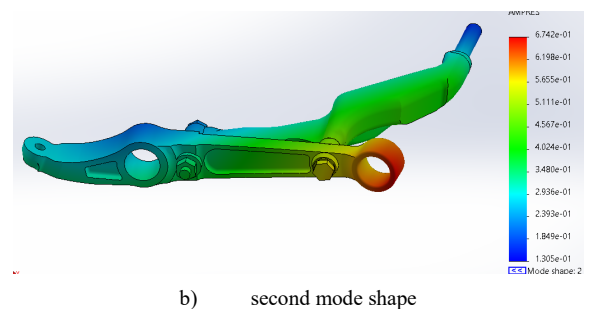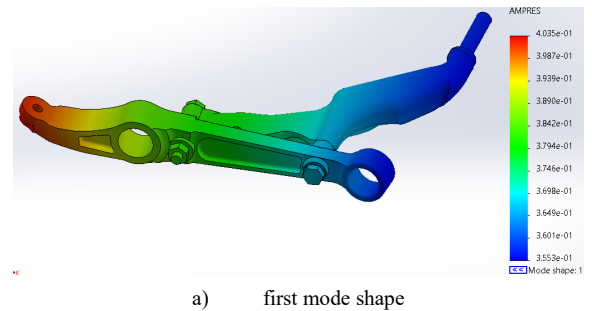
c)   third mode shape

Fig. 10.   Mode shapes.

C. Experimental results of Frequency Analysis

Fig. 11 presents the obtained experimental results for acceleration in raw format along the three axes - x, y, and z. The electrical signal received from the accelerometer was processed without software filtering.
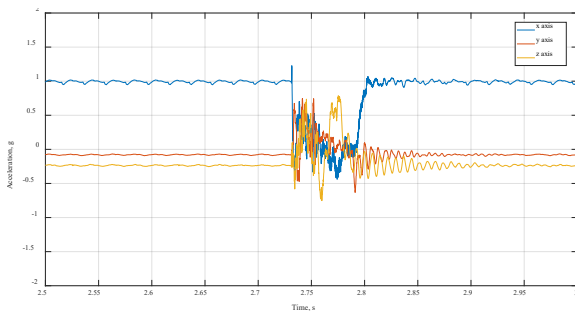

Fig. 11.   Experimental acceleration results.

FFT analysis of the experimental data was performed and at fig. 12 were presented results for the natural frequencies.
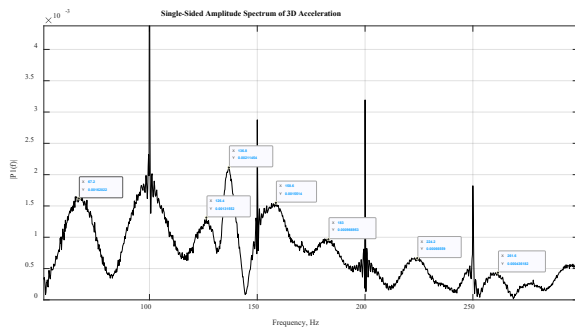

Fig. 12.   FFT analysis.

Table 6 presents the results regarding the natural frequencies obtained by FEA and results obtained experimentally.

TABLE 6 NATURAL FREQUENCY.

Mode number	FEA Natural frequency, Hz	Experimental Natural frequency, Hz
1	61.8	67.2
2	129.9	126.4
3	134.1	136.8
4	160.5	158.6
5	162.6	183
6	267.4	224.2

The results obtained of natural frequencies by FEA are comparable to those obtained experimentally.

IV.   CONCLUSIONS

Based on the performed study the following conclusions are made:

Using the geometric model of the support and the determined force values in various loading scenarios, a FEA was conducted within the SolidWorks Simulation environment. Significant for the strength analysis are the load Case I (maximum braking force) and load Case III (maximum force encountered when the car overcomes single obstacles). The largest stresses are obtained in the range 200 ÷ 240 MPa in the area of attachment of shock absorber, and the largest displacements in the range 8.3 ÷ 9.6 mm around of the hole for the ball joint.

To validate the FEA model developed for the lower arm of the front double wishbone suspension, an experimental frequency analysis was conducted, yielding results close to those obtained through FEA. The obtained results indicate that the lowest natural frequency of the lower arm is approximately 70 Hz, significantly higher than the frequency range of road surface irregularities (0 to 20 Hz). This supposes that when the vehicle is in motion, there will be minimal vibrations in the arm, preserving passenger comfort.

In a related study by the authors, the characteristics of rubber bushings of suspension were obtained. The use of this data and the elastic support fixation allows more realistic results to be obtained in the analyzes performed, which more accurately reflect the actual behavior of the lower arm of suspension.

The developed lower arm model, along with the study methodology and results, can be used for various types of analysis, for example topology optimization and fatigue assessment.

REFERENCES

[1] H. Dehkordi, Vibration and force analysis of lower arm of suspension system, Masters degree, Universite du Quebec, 2014.

[2] C. Ijagbemi, B. Oladapo at al., Design and simulation of fatigue analysis for a vehicle suspension system (VSS) and its effect on global warming, Procedia Engineering 159 (2016), doi: 10.1016/j.proeng.2016.08.135, pp. 124 - 132.

[3] Z. Georgiev and L. Kunchev, Study of the stresses in the front suspension components of a car passing over speed breakers, BulTrans2019, IOP Conf. Series: Materials Science and Engineering 664 (2019) 012012, doi:10.1088/1757-899X/664/1/012012.

[4] Z. Georgiev and L. Kunchev, Study of the vibrational behaviour of the components of a car suspension, MATEC Web of Conferences, 234 (2018), https://doi.org/10.1051/matecconf/201823402005.

[5] S. Abdullah, N.A. Kadhim, A. K. Ariffin, and M. Hosseini, Dynamic analysis of an automobile lower suspension arm using experiment and numerical technique, New Trends and Developments in Automotive System Engineering, pp. 231-248, 2011.

[6] V. Kulkarni, A. Jadhav, and P. Basker, Finite element analysis and topology optimization of lower arm of double wishbone suspension using Radioss and Optistruct, International Journal of

Science and Research, ISSN: 2319-7064, Vol. 3, Issue 5, pp. 639-643, 2014.

[7] A. Puranik, V. Bansode, S. Jadhav, and Y. Jadhav, Durability Analysis and optimization of an Automobile Lower Suspension Arm Using FEA and Experiment Technique, International Research Journal of Engineering and Technology (IRJET), e-ISSN: 2395-0056, p-ISSN: 2395-0072, Volume: 05 Issue: 09, pp. 1381-1389, 2018.

[8] V. Sajjanashettar, V. Siddhartha, at al., Numerical and experimental modal analysis of lower control arm for topography optimization, International Journal of Energy, Environment and Economics 27(1), ISSN: 1054-853X, pp. 17-31, 2019.

[9] H. Singh and G. Bhushan, Finite Element Analysis of a Front Lower Control Arm of LCV Using Radioss Linear, pp. 121-125, 2012, https://www.researchgate.net/publication/305355066.

[10] L. Tang, J. Wu, J. Lui, C. Jiang, and Shangguan, Topology optimization and performance calculation for control arms of a suspension, Advances in Mechanical Engineering, Volume 2014, Article ID 734568, 10 pages, https://dx.doi.org/10.1155/2014/734568.

[11] J. Marzbanrad and A. Hoseinpour, Structural optimization of MacPherson control arm under fatigue loading, Tehnički vjesnik 21, 3 (2017), pp.917-924, doi:10.17559/TV-20150225090554.

[12] M. Pachapuri, R. Lingannavar, N. Kelageri, and K. Phadate, Design and analysis of lower control arm of suspension system, The 3rd International Conference on Advances in Mechanical Engineering and Nanotechnology, Proceedings, Elsevier Ltd., Volume 47, Part 11, 2021, pp. 2949-2956, https://doi.org/10.1016/j.matpr.2021.05.035.

[13] S. Bhalshankar, Dynamic analysis of an lower control arm using harmonic excitation for investigation dynamic behaviour, PradnyaSurya Engineering Works, EasyChair Preprint №5933, 2021, https://easychair.org/publications/preprint/8G3j.

[14] J. Singh and S. Saha, Static structural analysis of suspension arm using finite element method, International Journal of Research in Engineering and Technology, eISSN: 2319-1163, 2015, Vol. 04, Issue 07, pp. 402-406.

[15] E. Morchev, Design and construction of the vehicle, Technica, Sofia, 1991.

[16] K. Ambarev, V. Nikolov, and S. Taneva, System for Experimental Determination of Natural Frequencies of Automotive Parts, 12th International Scientific Conference "TechSys 2023" – Engineering, Technologies and Systems, AIP Conf. Proc., (submitted for publication).

[17] S. Taneva, K. Ambarev, S. Penchev, and H. Atanasov, Frequency Analysis of an Arm of Macpherson Suspension on a Passenger Car, Proceedings of the 14th International Scientific and Practical Conference. Volume 3, pp. 252-256, Print ISSN 1691-5402, Online ISSN 2256-070X, https://doi.org/10.17770/etr2023vol3.7277.